Proceedings of Korean Nuclear Society Spring Meeting
Kori, Korea, May 2000

PROBABILISTIC RISK ASSESSMENT OF THE P-T LIMIT CURVES FOR PRESSURIZED WATER REACTORS: COOLDOWN CURVES

Changheui Jang, Ill-Seok Jeong, and Sung-Yull Hong

Korea Electric Power Research Institute
Nuclear Power Research Laboratory
103-16 Munji-dong, Yusong-gu
Taejon, Korea 305-380

ABSTRACT

During heatup and cooldown of pressurized water reactor, thermal stress was generated in the reactor pressure vessel (RPV) because of the temperature gradient. To prevent potential failure of vessel materials, pressure was required to be maintained below the P-T limit curves. In this paper, smaller reference flaws, reflecting advances in non-destructive evaluation technique, were assumed in constructing the P-T limit curves. The effect of reference flaw size on the maximum allowable pressure was not significant, especially at low temperature. The risks associated with the P-T limit curves, defined as flaw initiation and failure probabilities, were evaluated by the probabilistic fracture mechanics (PFM) technique. In PFM analysis, cladding was fully considered in such a way that the differences in thermal conductivity and thermal expansion coefficient were reflected in thermal and stress analysis. Also, the impacts of weld residual stress on the risk associated with P-T curves were evaluated. In summary, the effects of flaw sizes on the cooldown part of the P-T limit curves and associated risks were not so significant. Finally, the potential of incorporation of flaw orientation in constructing the P-T limit curves was evaluated. It was found that full consideration of flaw orientation results in comparable risks for both axial and circumferential flaws.

1. INTRODUCTION

A Reactor pressure vessel (RPV) is the most critical component in nuclear power plants, housing reactor core and comprising a part of primary system pressure boundary. Naturally, its structural integrity gravely affects overall plant safety, and plant lifetime management including plant life extension. Because of its proximity to reactor core, RPV is subjected to

radiation embrittlement due to high fast neutron fluence, losing ductility and fracture toughness. Radiation embrittlement is characterized as the combination of reduction in Charpy upper shelf energy (USE) and increase in reference temperature-nil ductility transition (RT_{NDT}). The beltline region of RPV is especially prone to embrittlement due to high fast neutron fluence and, usually, the existence of welds. To ensure safety, USE and RT_{NDT} should meet well defined criteria specified in the regulatory requirement [1,2].

During heatup/cooldown process of the primary coolant system, coolant temperature and pressure were required to be appropriately controlled to ensure that the structural integrity of RPV is maintained. Current regulation requires that pressure and temperature should be limited by P-T limit curves constructed in accordance to 10CFR50 App. G [1] and ASME Sec. XI App. G [3]. The method is based on linear elastic fracture mechanics assuming a relatively large reference flaw, or 1/4th of the thickness of RPV, on the surface. Recently, a risk informed flaw tolerance approach was applied in an effort to relax the P-T limit curves [4]. Also, the appropriateness of such a large reference flaw is being questioned resulting from the advances in non-destructive evaluation techniques. The applicability of smaller reference flaw was also explored [5].

In this paper, the risks associated with the P-T limit curves are examined using probabilistic fracture mechanics (PFM) technique [6,7]. First, an alternative method used in this study to construct the P-T limit curves is explained and compared with the current method specified in ASME App. G. Next, series of the P-T limit curves assuming different flaw sizes, ranging from 1/4 to 1/10 of the thickness of the RPV, were constructed while satisfying the basic philosophy of App. G methodology. The risks associated with the P-T limit curves were quantified using PFM technique. In evaluating the risks, the existence of stainless steel cladding was fully incorporated in such a way that differences in thermal conductivity and thermal expansion coefficient were reflected in thermal and stress analysis [8]. Also, the potential impacts of weld residual stress [5,9] on the risk associated with P-T curves were evaluated. Finally, the effects of adopting ASME Code Case N-588 [10] in constructing the P-T limit curves were evaluated quantitatively.

2. CONSTRUCTION OF P-T LIMIT CURVES

2.1 Appendix G Method

Current ASME Section XI, Non-mandatory Appendix G "Fracture Toughness Criteria for Protection Against Failure" provides the basis and procedure for constructing P-T limit curves applicable to light water reactors [3]. The procedure is based on the principles of linear elastic fracture mechanics, assuming a semi-elliptical surface flaw with the depth of one fourth of the thickness of the vessel and the length of six times the depth. To prevent brittle failure of the vessel, the mode I stress intensity factor, defined as the sum of the stress intensity factors (K_I) from thermal loading and two times of pressure loading, should be lower than the reference fracture toughness, or K_{IR} given as a function of temperature and RT_{NDT}.

During cooldown, K_I corresponding to membrane tension for the postulated axial defect, K_{Im} is given as follows (converted to SI units);

$$
\begin{aligned}
&K_{Im} = M_m \cdot (p \cdot R_i / t) \\
&\text{where } M_m = 0.2954 \qquad \text{for t} < 0.1016 \\
&\qquad M_m = 0.9267\sqrt{\text{t}} \quad \text{for } 0.1016 \le \text{t} \le 0.3048 \\
&\qquad M_m = 0.5116 \qquad \text{for } 0.3048 < \text{t} \\
&\qquad p = \text{internal pressure (MPa)} \\
&\qquad R_i = \text{vessel inner radius (m)} \\
&\qquad t = \text{vessel wall thickness (m)}
\end{aligned}
\qquad \text{Eq. 1)}
$$

The maximum K_I produced by a radial thermal gradient for a postulated axial inside surface defect, K_{It} is given as follows (converted to SI units);

$$K_{It} = 18.353 \cdot CR \cdot t^{2.5}$$

$$\text{where } CR = \text{cooldown rate (C/hr)} \qquad \text{Eq. 2)}$$

The through-wall temperature difference associated with the maximum thermal K_{Im} can be determined graphically using figures provided in App. G. The requirement to be satisfied is as follows;

$$2 \cdot K_{Im} + K_{It} < K_{IR} \qquad \text{Eq. 3)}$$

Using equations 1) through 3) and appropriate figures in the App. G, the maximum allowable pressure during the cooldown process, characterized as CR in equation 2), can be calculated easily.

2.2 Alternative Methods

Beltline region of RPV is sufficiently far away from the nozzle area as well as the upper and lower head to be treated as axi-symmetric infinite cylindrical shell during the heat transfer/conduction analysis. In axi-symmetric infinite cylinder, heat transfer occurs only in r-direction. This can considerably simplify the analysis. Convective boundary condition and unsteady heat conduction equations given below should be solved to find the time dependent temperature profile, T(r,t).

$$-k(t) \cdot \left. \frac{T(r,t)}{\partial r} \right|_{wall} = h(t) \cdot (T_{wall}(t) - T_{\infty}(t)) \qquad \text{Eq. 4)}$$

$$\frac{1}{r} \frac{\partial}{\partial r} \left(r \frac{\partial T(r,t)}{\partial r} \right) = \frac{1}{\alpha(t)} \cdot \frac{\partial T(r,t)}{\partial t} \qquad \text{Eq. 5)}$$

General solutions of equation 5) are provided as Bessel functions for special boundary condition of abrupt change of T_{wall}. But for time dependent boundary condition like equation 5), closed form solutions are hard to be found. Therefore, numerical solutions are found using finite element method in most practical cases [6]. Once the temperature profile has been found, it could be approximated as a fourth-order polynomial. Similarly, thermal stress arising from the temperature distribution can be calculated and subsequently approximated as a third-order polynomial as follows;

$$\sigma_{base}(x,t) = \frac{E_{base}}{1-\nu_{base}} \cdot (T_{ref}(t) - T_{base}(x,t)) \cdot \alpha_{base}$$
$$= \sum_{i=0}^{3} C_i(t) \cdot x^i \qquad \text{Eq. 6)}$$

As shown in equation 6), coefficients of stress formula are directly derived from those of temperature profile. Once stress distribution from $T_{base}(x,t)$ was determined from equation 6), additional stress due to the existence of cladding had to be determined. There are two sources of cladding stress. One is the stress from the difference in thermal expansion between clad and base metals. The other is the stress from the difference between real temperature in clad, T(x,t) and hypothetical temperature extrapolated from $T_{base}(x,t)$ [8].

For a stress distribution given as polynomial functions, corresponding stress intensity factor could be found as follows;

$$K_{Ji} = \sqrt{\pi a W} \cdot \sum_{n=0}^{N} C_n F_n a^n \qquad \text{Eq. 7)}$$

where C_n is the coefficient of each term in stress distribution shown in equation 6), and F_n is defined as weight function for each terms in stress distribution and depends on variety of factors like geometry, aspect ratio, flaw orientation, and flaw depth. For an infinitely long eccentric cylinder with radius to thickness ratio (R/t) of 10, weight functions are given in many publications [11-15]. Appropriate weight functions can be used to calculate by polynomial fitting of the published values.

Therefore, stress intensity factors resulting from the temperature distribution, which correspond to K_{It} in equation 2), can be found using equations 6) and 7). Once K_{It} has been calculated, the maximum allowable stress can be calculated using equation 1) and 3) as current App. G method.

2.3 Justification of the Alternative Method

A hypothetical reactor pressure vessel was considered to compare the P-T limit curves per ASME App. G method and the alternative method used in this study. Assumed RPV is typical Westinghouse 2-loop design with inner radius of 1676 mm, thickness of 165 mm, and clad with stainless steel of 4.2 mm thick. The material properties of the vessel are summarized in table 1. It should be noted that only the material properties of the base metal were used for the comparison, because the current App. G method does not explicitly

Table 1. Thermo-mechanical properties of the RPV

Material Property	Carbon Steel (Base & Weld)	Stainless steel cladding
Thermal Conductivity, W/m-℃	40.897	17.238
Specific Heat, KJ/Kg-℃	0.5091	0.5259
Density, Kg/m^3	7809.5	7851.0
Modulus of Elasticity, GPa	182.85	185.26
Thermal Expansion Coefficient, m/m-℃	13.29E-6	17.12E-6
Poisson's Ratio	0.3	0.3

consider stainless steel cladding in the P-T limit curve construction. The resulting P-T curves, constructed assuming RT_{NDT} = 67.2°C, are shown in figure 1. As shown in the figure, both methods produced similar P-T limit curves, though current method allowed slightly higher pressure at the same coolant temperature.

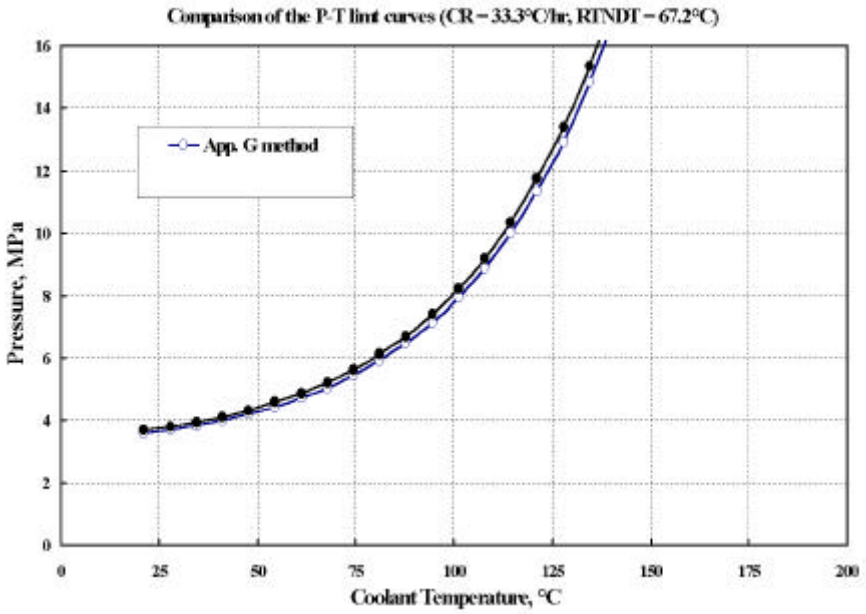

Figure 1. Comparison of the P-T limit curves constructed using App. G method and the alternative method

3. RISK ASSOCIATED WITH P-T LIMIT CURVES

3.1 P-T Limit Curves for Various Flaw Sizes

Again, a typical Westinghouse 2-loop RPV, whose material properties are shown in table 1, is assumed for the analysis. The radiation embrittlement characteristics are summarized in table 2. Reference flaws were varied from 1/4T to 1/10T with semi-elliptical shape with

Table 2. Radiation embrittlement related properties of the RPV: mean and standard deviation.

Parameters	Mean Value	Std. Dev.
Copper Content, w/o	0.29	0.07
Nickel Content, w/o	0.68	0.05
Initial RT_{NDT}, °C	-32.8 °C	0
RTNDT Shift Equation	Reg. Guide 1.99 Rev. 2	15.6 °C
Fluence at RPV inner surface	3.00 x1019/cm2	0.16
Errors in KIC Reference Curve	ASME derived mean	0.15
Errors in KIA Reference Curve	ASME derived mean	0.1
Flux Attenuation, /m	9.45	

depth to length ratio of 1/6. The cooldown part of the P-T limit curves constructed for various reference flaws by alternative method are shown in figure 2. The effect of reference flaw size is not so significant at lower part of the curves. However, for the upper part of the curves, the maximum allowable pressures become lower as the reference flaw size increased.

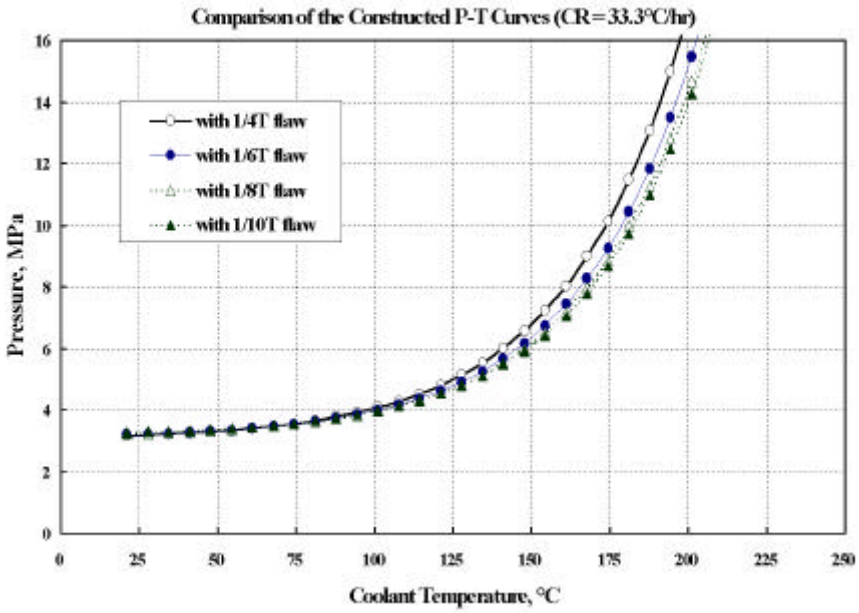

Figure 2. Comparison of the P-T limit curves constructed assuming various flaw sizes using the alternative method.

3.2 Risks Associated with the P-T Limit Curves

The probabilistic fracture mechanics analyses were performed for the P-T limit curves shown in figure 2. The overall flow of the probabilistic fracture mechanics analysis is shown in figure 3. From the given pressure and temperature curves, thermal and stress analyses, and stress intensity factor calculation are performed. Especially, as shown in figure 4, the residual stress distribution was approximated as a third-order polynomial using published studies [5,9].

For given vessels, fast neutron fluence, flaw size, Cu and Ni contents, error in RT_{NDT}, and finally fracture toughness values are simulated with the means and standard deviations provided in table 2. The fracture toughness values are then compared to the applied stress intensity factors to check whether the flaws initiate and propagate through the RPV wall. The risk was calculated as two ways, such as initiation probability that is the number of initiation divided by the number of simulated vessels, and failure probability that is the number of failure divided by the number of simulated vessels. It should be noted that once initiated the flaws were treated as infinite flaws. Also, if initiated flaw grew over 75% of the thickness of the vessels, it was considered a failure.

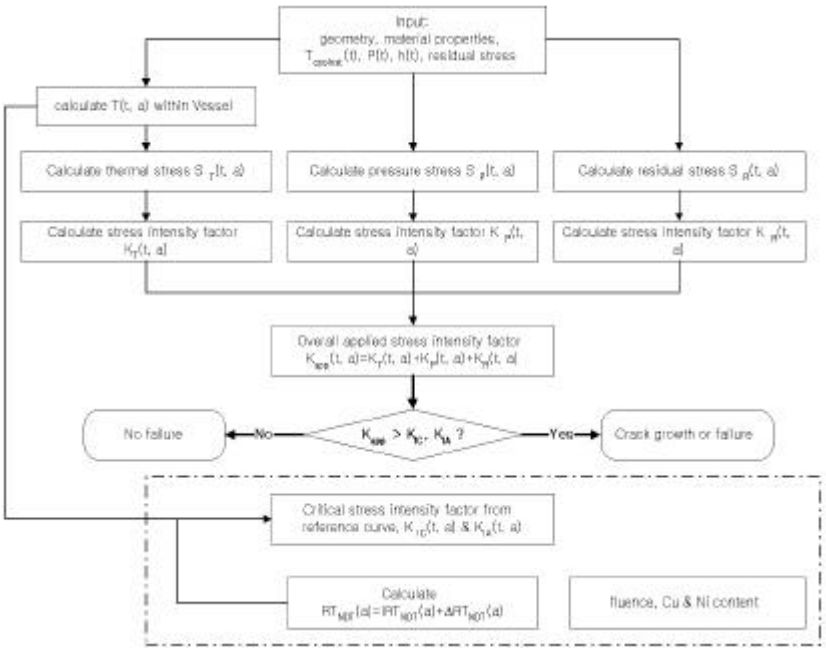

Figure 3. Schematics of probabilistic fracture mechanics analysis

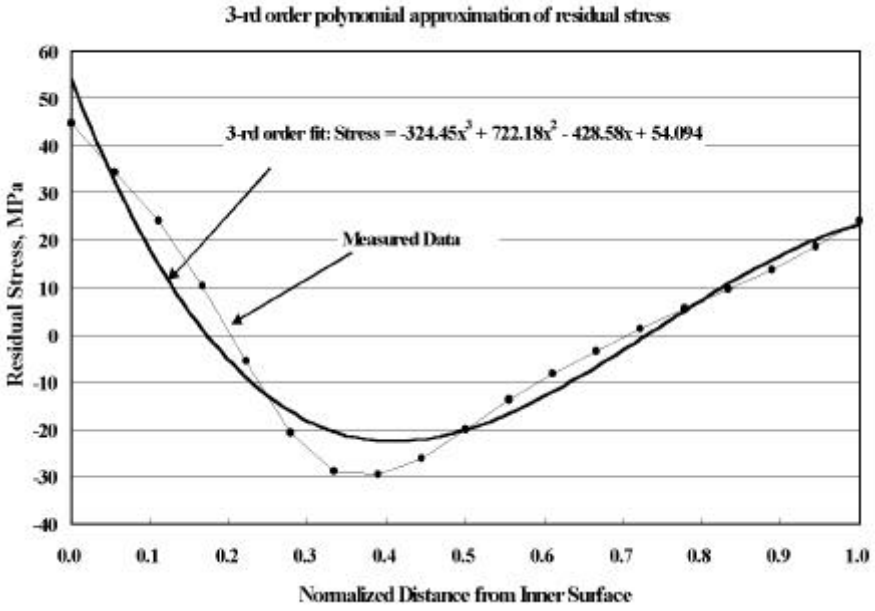

Figure 4. Comparison of the measured residual stress distribution and 3-rd order polynomial approximation.

The risks were calculated for the following cases, for both axial and circumferential flaws;
Case S-0: Residual stress ignored and a semi-elliptical flaw with discrete size assumed

Case S-R: Residual stress considered and a semi-elliptical flaw with discrete size assumed

Case M-0: Residual stress ignored and a semi-elliptical flaw with Marshall distribution assumed

Case M-R: Residual stress considered and a semi-elliptical flaw with Marshall distribution assumed

Case S-0

Up to a million simulations, neither initiation or failure happened for both flaw orientations.

Case S-R

The results are summarized in table 3. Though initiation occurred for both flaw orientations, their probabilities were less than 10^{-5}. For both flaw orientations, no failure occurred up to a million simulations.

Table 3. Flaw initiation and failure probabilities depending on the reference flaw size (residual stress assumed, with a single discrete flaw size)

Reference Flaw size	axial flaws		circumferential flaws	
	Initiation P	Failure P	Initiation P	Failure P
1/4T	< E-6	< E-6	< E-6	< E-6
1/6T	2.00E-6	< E-6	< E-6	< E-6
1/8T	6.00E-6	< E-6	2.00E-6	< E-6
1/10T	< E-6	< E-6	< E-6	< E-6

Case M-0

The results are summarized in table 4. Compared to table 3, initiation probability increased substantially by assuming Marshall flaw distribution. For axial and circumferential flaws, flaw initiation probabilities were virtually unchanged as the reference flaw size decreases. The initiation probabilities for the circumferential flaws are about half of those for the axial flaws. For both flaw orientations, no failure occurred up to a million simulations.

Table 4. Flaw initiation and failure probabilities depending on the reference flaw size (no residual stress, with a flaw with Marshall distribution)

Reference Flaw size	axial flaws			circumferential flaws		
	Initiation P	ratio	Failure P	Initiation P	ratio	Failure P
1/4T	6.32E-3	1.00	< E-6	3.25E-3	1.00	< E-6
1/6T	6.37E-3	1.01	< E-6	3.20E-3	0.98	< E-6
1/8T	6.46E-3	1.02	< E-6	3.28E-3	1.01	< E-6
1/10T	6.53E-3	1.03	< E-6	3.31E-3	1.02	< E-6

Case M-R

The results are summarized in table 5. As for Case M-0, flaw initiation probabilities were virtually unchanged with reference flaw size. Also, the initiation probabilities for the circumferential flaws were consistently lower than those for the axial flaws. Also, the initiation probabilities increased to about 3.5 times (axial flaws) to 4.4 times (circumferential flaws) by incorporating residual stress. The failure probabilities for the axial flaws increased by about 60% when reference flaw size decreases from 1/4T to 1/10T. This could be attributed to about 0.05 0.1 MPa higher allowable pressure for 1/10T flaws than 1/4T flaws on the lower part of the curves, where most initiations and failures occurred. No failure happened up to a million simulations for the circumferential flaws.

Table 5. Flaw initiation and failure probabilities depending on the reference flaw size (residual stress assumed, with a flaw with Marshall distribution)

Reference	axial flaws				circumferential flaws		
Flaw size	Initiation P	ratio	Failure P	ratio	Initiation P	ratio	Failure P
1/4T	2.27E-2	1.00	1.56E-4	1.00	1.41E-2	1.00	< E-6
1/6T	2.28E-2	1.00	1.84E-4	1.18	1.44E-2	1.02	< E-6
1/8T	2.30E-2	1.01	2.40E-4	1.54	1.45E-2	1.03	< E-6
1/10T	2.33E-2	1.03	2.50E-4	1.60	1.46E-2	1.04	< E-6

3.3 Summary of the Effects of Reference Flaw Size

When a discrete flaw was assumed, initiation probabilities were less than 10^{-5} and failure probabilities were less than 10^{-6} even with the residual stress incorporated. Assuming a Marshall flaw distribution substantially increased initiation probabilities. Incorporation of residual stress further increased flaw initiation probabilities by 3.5 - 4.4 times depending on the flaw orientation. The effect of residual stress seems even greater for the failure probabilities, increasing from less than 10^{-6} to the order of 10^{-4} for the axial flaws for the range of reference flaw sizes. It is evident that the risks associated with the P-T limit curves are consistently lower for the circumferential flaws compared to those for the axial flaws. The difference become even greater for the failure probabilities, in such that failure probabilities for circumferential flaws are less than 10^{-6} for all conditions explored in this paper.

4. INCORPORATION OF CODE CASE N-588

As mentioned above, the risks associated with the P-T limit curves are considerably lower for the circumferential flaws that those for the axial flaws. This could be the result of the current requirement that the P-T limit curves be constructed assuming axially oriented flaw regardless of the characteristic of the relevant RPVs. When the effects of flaw orientation is considered in calculating the applied stress intensity factors acting on the tip of the 1/4T semi-elliptical flaws, the stress intensity factors for the circumferential flaws were considerably

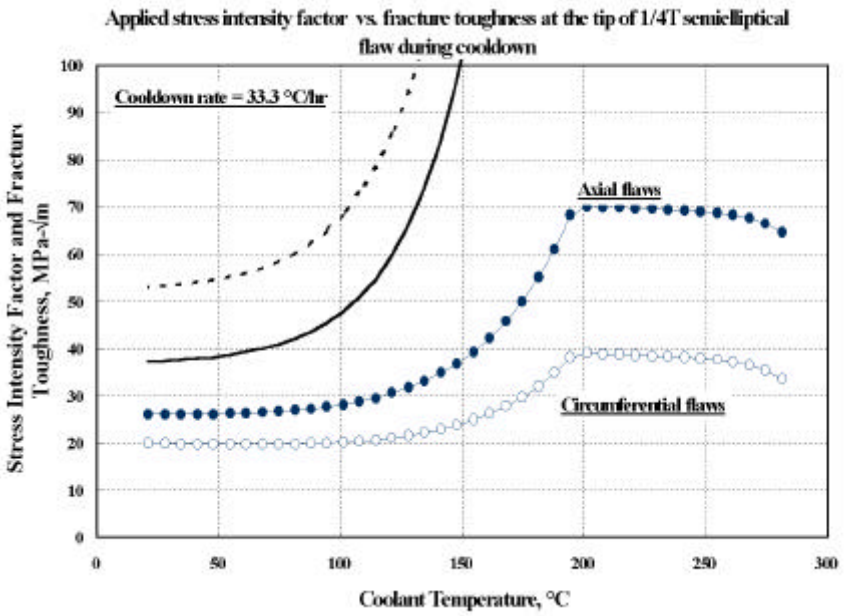

Figure 5. Comparison of applied stress intensity factors at the tip of axial and circumferential flaws with fracture toughness.

lower than those for the axial flaws, as shown in figure 5. Also, recently, a Code Case [10] was introduced to deal with this issue by giving credit of, mostly, reduced effects of pressure loading for the circumferentially oriented flaws. The P-T limit curves were constructed while considering the orientation of reference flaws, and shown in figure 6. As shown in the figure, incorporation of the flaw orientation resulted in about two-fold increase in the maximum allowable pressure in the P-T limit curves for circumferential flaws.

For the P-T limit curves incorporating flaw orientation effects, the risks were evaluated for the four cases previously specified and summarized in table 6. As shown in the table, in all four cases, the initiation probabilities for the circumferential flaws are comparable or less than those for axial flaws, even with the about twice of the allowable pressure at the same temperatures. Still, the failure probabilities for the circumferential flaws are far less than those for axial flaws.

5. SUMMARY AND DISCUSSION

Considering that RPVs are rigorously inspected before and during the operation of the nuclear power plants, and substantial improvement in non-destructive evaluation for detecting and measuring the flaws within the RPVs, it is hard to conceive that any large flaws are unnoticed. Reflecting such argument, the effects of the smaller reference flaws on the P-T limit curves for cooldown were examined. Despite of the decrease in applied stress intensity factors at the tip of the flaws, changes in the maximum allowable pressures are not so significant for cooldown curves. This could be the result of increased RT_{NDT}s due to higher

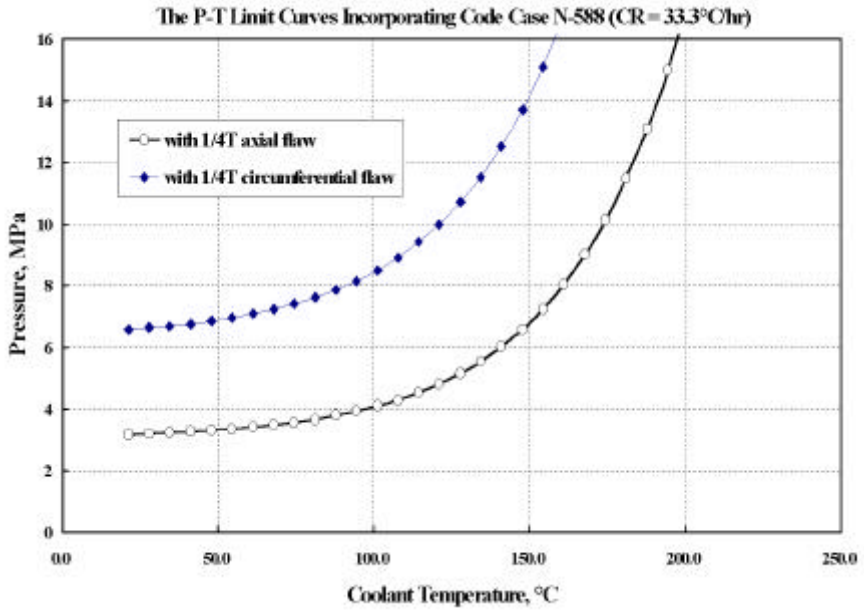

Figure 6. Comparison of P-T limit curves incorporating the flaw orientation effect

Table 6. Comparison of flaw initiation and failure probability of axial and circumferential flaws when Code Case N-588 is applied

Condition		axial flaws			circumferential flaws		
Flaw	Residual stress	Initiation P	ratio	Failure P	Initiation P	ratio	Failure P
Single	No	< E-6	< E-6	< E-6	-	< E-6	-
Single	Yes	< E-6	< E-6	< E-6	-	< E-6	-
Marshall	No	6.32E-3	< E-6	5.44E-3	0.86	< E-6	-
Marshall	Yes	2.27E-2	1.56E-4	2.14E-2	0.94	1.00E-6	0.01

fluence at the tip of smaller reference flaws. However, for the heatup curves, where outer surface flaws are assumed, it is expected that the maximum allowable pressures increase somewhat, as both the applied stress intensity factors and RT_{NDT}s decrease at the same time.

The risks associated with the P-T limit curves were quantitatively evaluated using PFM technique. When residual stresses are not considered, neither flaw initiation nor failure happened regardless of the orientation of the flaw (a single reference flaw at the inner surface of the RPV) used in PFM.

Assuming Marshall flaw distribution resulted in greater flaw initiation probabilities and failure probabilities than when a single discrete flaw was assumed. This is the result of increased probabilities of small flaws existing near the inner surface where fracture toughness of the materials are low.

In all four cases considered in the study, failure probabilities of circumferential flaws are

consistently lower than 10^{-6}. This translates that application of axial flaw-based P-T limit curves could be overly conservative for the RPVs where the critical materials are circumferential welds.

This point is confirmed again when flaw orientation is considered in constructing the P-T limit curves as described in ASME Code Case N-588. Despite of about two-fold increase in pressure, the risks, both initiation and failure probabilities, associated with the P-T limit curves for the circumferential flaws are comparable or lower that those for the axial flaws. This could be used to confirm the appropriateness of Code Case N-588 with the information on the risks associated with the P-T limit curves.

6. CONCLUSIONS

Probabilistic aspects of the cooldown part of the P-T limit curves were evaluated using probabilistic fracture mechanics technique.

The impacts of the smaller reference flaw sizes are explored and found that

- the resulting P-T limits curves are not much affected by the reference flaws sizes assumed, and
- the probabilistic evaluation resulted in virtually the same initiation probabilities as the reference flaw size decreases, even when the residual stress is considered, and
- when residual stress was incorporated and Marshall flaw distribution was assumed, the failure probabilities for the axial flaws increased by about 60% as reference flaw size decreases from 1/4T to 1/10T, and
- for the RPVs whose controlling materials are circumferential welds, the P-T limit curves constructed assuming axial flaws are overly conservative from the risk point of view.

When flaw orientation is incorporated in constructing the P-T limit curves,

- the maximum allowable pressures for the circumferential flaws increased about two-fold, and
- the risks associated with the P-T limit curves become comparable for both flaw orientations.

Though this study is limited to the cooldown part of the P-T limit curves, same approach can be used for the heatup part of the curves.

REFERENCES

1. USNRC, Fracture Toughness Requirements, Code of Federal Regulation 10CFR50 App. G, 1995
2. USNRC, Fracture Toughness Requirements for Protection against Pressurized Thermal Shock Events, Code of Federal Regulation 10CFR50.61, 1995.
3. ASME, Fracture Toughness Criteria for Protection Against Failure, ASME Section XI Nonmandatory Appendix G, 1995.
4. R. M. Gamble, A Risk-Informed Flaw Tolerance Approach for Increasing ASME Section XI, Appendix G PT Limits, EPRI TR-107451, 1997.

5. T. Dickson, B. R Bass, and W. J. McAfee, "The Inclusion of Weld Residual Stress in Fracture Margin Assessments of Embrittled Nuclear Reactor Pressure Vessels," PVP-373, pp. 387-395, 1998.
6. R. D. Cheverton and D. G.Ball, OCA-P, A Deterministic and Probabilistic Fracture-Mechanics Code for Application to Pressure Vessels, Oak Ridge National Laboratory, NUREG/CR-3618 (ORNL-5991), 1984.
7. F. A. Simonen et al., 1986, VISA-II, A Computer Code for Predicting the Probability of Reactor Vessel Failure, Battelle Pacific Northwest Laboratories, USNRC Report NUREG/CR-4486, 1986.
8. C. H. Jang, Treatment of Cladding in Pressurized Thermal Shock Evaluation, KEPRI Report TM.96NJ12.P1998.898, 1998.
9. F. A. Simonen, and K. I. Johnson, "Effects of Residual Stresses and Underclad Flaws on the Reliability of Reactor Pressure Vessels," PVP-251, pp. 101 113, 1993.
10. ASME, Alternative to Reference Flaw Orientation of Appendix G for Circumferential Welds in Reactor Vessels, ASME Section XI Nuclear Code Case N-588, 1998.
11. I. S. Raju and J. C. Newman, Jr., "Stress-Intensity Factors for Internal and External Surface Cracks in Cylindrical Vessels," J. of Pressure Vessel Technology, Vol. 104, pp.293-298, 1982.
12. I. S. Raju and J. C. Newman, Jr., "Stress-Intensity Factors for Circumferential Surface Cracks in Pipes and Rods under Tension and Bending Loads," in Fracture Mechanics: Seventeenth Volume, ASTM STP 905, ASTM, Philadelphia, pp. 789-805, 1986.
13. J. A. Keeney and J. W. Bryson, "Stress-Intensity-Factor Influence Coefficients for Semielliptical Inner Surface Flaws in Clad Pressure Vessels," in Fracture Mechanics: 26th Volume, ASTM STP 1256, ASTM, Philadelphia, 1995.
14. X. Wu and A. J. Carlsson, Weight Functions and Stress Intensity Factor Solutions, Pergamon Press, Oxford, 1991.
15. T. Fett and D. Munz, Stress Intensity Factors and Weight Functions, Computational Mechanics Publication, Boston, 1997.